Front. Earth Sci.
https://doi.org/10.1007/s11707-019-0798-0

RESEARCH ARTICLE

Improvement of typhoon rainfall prediction based on optimization of the Kain-Fritsch convection parameterization scheme using a micro-genetic algorithm

Jia ZHU[1,2], Jiong SHU (✉)[1,2], Xing YU[3]

1 Key Laboratory of Geographic Information Science (Ministry of Education), East China Normal University, Shanghai 200241, China
2 School of Geographic Sciences, East China Normal University, Shanghai 200241, China
3 Beijing Thematic Technology Co., Ltd., Beijing 100020, China

Abstract Inclusion of cloud processes is essential for precipitation prediction with a numerical weather prediction model. However, convective parameterization contains numerous parameters whose values are in large uncertainties. In particular, it is still not clear how the parameters of a sub-grid-scale convection scheme can be modified to improve high-resolution precipitation prediction. To address these issues, a micro-genetic (micro-GA) algorithm is coupled to the Kain-Fritsch (KF) convective parameterization scheme (CPS) in the WRF to improve the quantitative precipitation forecast (QPF). The optimization focuses on two parameters in the KF scheme: the convective time scale and the conversion rate. The optimizing process is controlled by the micro-GA using a QPF skill score as the fitness function. Two heavy rainfall events related to typhoons that made landfall over the south-east coastal region of China are selected, and for each case the parameter values are adjusted to achieve the best QPF skill. Significant improvements in QPF are evident with an increase in the average equitable threat score (*ETS*) by 5.8% for the first case, and by 18.4% for the second case. The results demonstrate that the micro-GA-KF coupling system is effective in optimizing the parameter values, which affect the applicability of CPS in a high-resolution model, and therefore improves the rainfall prediction in both *ETS* and spatial distribution.

Keywords quantitative precipitation forecast, micro-GA, Kain-Fritsch scheme, typhoon

Received May 17, 2019; accepted October 7, 2019

E-mail: jshu@geo.ecnu.edu.cn

1 Introduction

Typhoons accompanied by severe convective weather cause flooding and societal damage over coastal areas worldwide. Numerical models have been widely used to investigate typhoon evolution. Despite the improvement of numerical weather prediction (NWP) in recent decades (Bauer et al., 2015), the prediction of precipitation in terms of intensity and location remains challenging, as cumulus convection, cloud microphysics, and planetary boundary layer turbulence are often poorly resolved or parameterized by numerical models (Dai, 2006; Qiao and Liang, 2016). The convective parameterization scheme (CPS) that controls sub-grid-scale convective processes plays a particularly important role in regulating the pattern of, and temporal variation in, predicted typhoon precipitation (Arakawa, 2004; Liang et al., 2007). In recent decades, numerous CPSs have been developed and integrated into mesoscale models (Zheng et al., 2016). Many studies have demonstrated that tropical cyclone precipitation is sensitive to the choice of CPS (Yang and Tung, 2003; Li and Pu, 2009; Sun et al., 2014; Zhang and Wang, 2018). In simulations at a relatively coarse resolution greater than about 25 km, the use of a CPS is necessary to properly express latent heat release and vertical fluxes in convective columns. However, in experiments with a smaller grid-scale (less than 10 km) this remains a controversial issue as the convective eddies can be explicitly solved by the models themselves (Li et al., 2018). Davis and Bosart (2002) conducted a typhoon simulation using a 9 km grid-scale outer nest and 3 km grid-scale innermost nest, with and without CPS, to assess the influence of grid spacing and CPS on typhoon intensification. Sugimoto and Takahashi (2016) assessed the influence of horizontal grid-scale and the CPS on regional-scale precipitation over

South Asia using the WRF model, reporting that smaller grid-scale without a CPS improved the spatial distribution of monthly precipitation. Further research (Li et al., 2018) has shown that for Typhoon Haiyan (2013), a 2 km grid-scale with no CPS or a 4 km grid-scale with CPS facilitated simulating the tracks, intensities, and structures. Nevertheless, the effect of CPSs in smaller grids has not been explored in depth. The above studies only compared the performance of the CPS as an integral "black box" without explicitly identifying the constituent element that causes the difference in simulations (Neggers et al., 2004).

To use a CPS at high resolution effectively, it is essential to examine accurately the values of different functions in the parameterization scheme for convective precipitation. Therefore, optimizing parameters in the CPS is a possible way to improve numerical forecasts of typhoons with smaller grids. Therefore, the focus of the problem is whether appropriate values of several important parameters that meet the basic assumptions and closure assumptions can be found in the 2–10 km resolution range termed the "grey zone." According to Li (2013), simulations of 20 typhoons in the north-west Pacific Ocean from 2003 to 2008 showed that the simulation of typhoon path and intensity is very sensitive to the selection of CPS, and that the Kain-Fritsch (KF) scheme gives the best simulations. Based on the convective cloud depth and convective velocity scale, the convective adjustment time scale (T_{con}) in the KF scheme has been modified to improve simulations of precipitation with 12- and 36-km model grid spacing (Bullock et al., 2015). Also, the grid-scale rainfall is dependent on the hydrometeor feedback, which is affected by the conversion rate (Correia et al., 2008). Thus, the problem of CPS parameter optimization is transformed into the optimization of two parameters in the KF scheme — the T_{con} and the conversion rate (c) — because of the relatively large uncertainties at a high resolution.

When considering adaptive selections for parameter values, the genetic algorithm (GA) is a likely choice because of its success in solving problems like atmospheric parameters forecast, global solar radiation prediction, land surface temperature retrieving and so on (Aybar-Ruiz et al., 2016; Singh et al., 2016). The GA is easy to implement and effective in finding improved parameter values; furthermore, the micro-GA algorithm is reasonably efficient and does not require excessive computational resources (Lee et al., 2006; Yu et al., 2013). Lee et al. (2006) improved the quantitative precipitation forecast (QPF) in a heavy rainfall case in Korea by optimizing the reduction rate of the convective available potential energy in the KF scheme, and the computational parameter in Fifth-Generation Penn State/NCAR Mesoscale Model (MM5) with a standard GA. On this basis, optimization by micro-GA of two parameters (T_{con} and c) in the KF WRF scheme has improved the QPF of Typhoon Rusa in South Korea (Yu et al., 2013).

In addition, cloud processes are expounded implicitly and explicitly in the WRF model using the CPS and cloud microphysics scheme (MPS). Both these schemes not only manage the spatial and temporal distribution of precipitation but also conduce to the expression of convection in the model (Sandeep et al., 2018). Therefore, the optimal selection of parameters in the KF scheme and different MPSs for better prediction of convective typhoon precipitation at the selected spatial scale of 10 km resolution should also be studied and the use of a CPS should not be excluded.

This study investigates the improvement of the QPF skill of typhoons in the WRF, a state-of-the-art NWP, focusing on the optimization of the KF scheme with micro-GA. The remainder of this paper is organized as follows. Typhoon cases and validation data are briefly described in Section 2. Section 3 illustrates the model formulation, the KF scheme, the micro-GA method and the optimization process. Results and a discussion are presented in Section 4.

2 Typhoon cases and observational data

2.1 Synoptic history of typhoon cases

As shown in Fig. 1(a), Typhoon Meranti (2016) was detected as a tropical cyclone over the Western North Pacific (WNP) at 0600 UTC 10 September 2016, before developing into a tropical storm. Tracking to the west-north-west, the tropical storm continued to strengthen to a typhoon until 1800 UTC 11 September. It then strengthened rapidly and became a super typhoon early on 12 September. Meranti reached its peak at 1200 UTC 13 September, with a minimum sea level pressure (MSLP) of 890 hPa and maximum wind speed of 75 m/s. At 0900 UTC 14 September, Super Typhoon Meranti passed to the southern Taiwan, China and then weakened to a strong typhoon as a result of land interaction. At 1900 UTC 14 September, Meranti made landfall in Xiamen, Fujian, China and then continue to move in the direction of north-west and north. The cloud and rain system affected 11 provinces and cities in East China after it made landfall. Following extratropical transition, Meranti rapidly weakened to an extratropical cyclone the next day, and dissipated shortly after passing to the south of the Korean Peninsula. Meranti caused severe economic losses and casualties in eastern China due to torrential rainfall with 24-h precipitation amounts to 200 mm (Li et al., 2019).

As shown in Fig. 1(b), a tropical disturbance developed on 27 September 2013 over the West Pacific Ocean off the northern coast of Palau and began to move north-west. On 29 September, this strengthening tropical disturbance was categorized as the 22nd tropical depression of the 2013 pacific typhoon season. Keep moving to the north-west, the tropical depression continued to strengthen and became

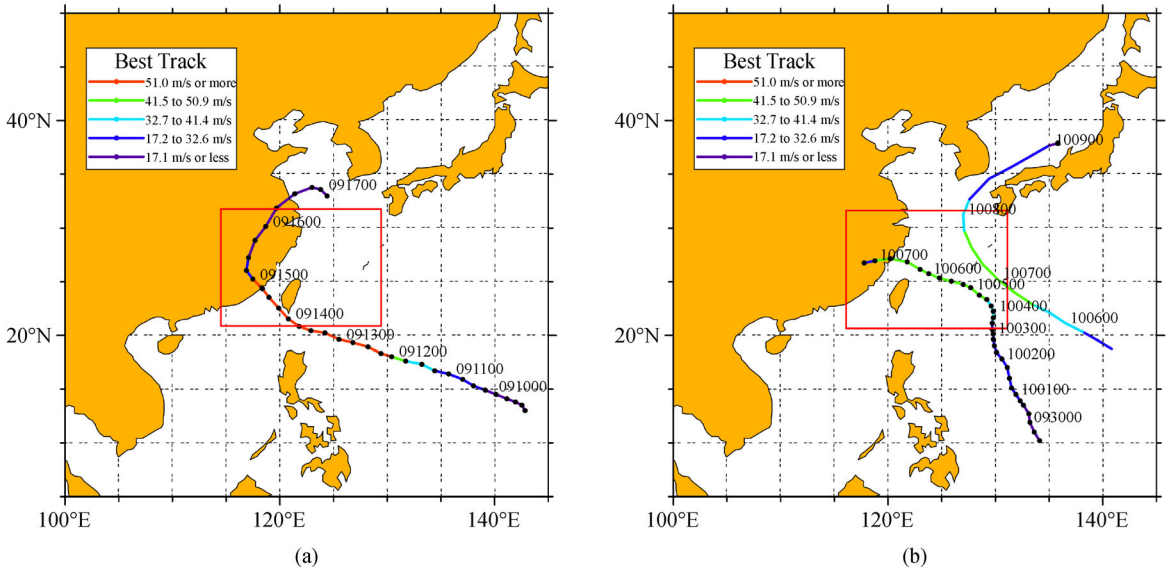

Fig. 1 Typhoon track, simulation domain (red rectangle): (a) for Meranti, (b) for Fitow (left) and Danas (right).

the better-organized tropical storm Fitow with maximum sustained wind of 18 m/s. Fitow was strengthening rapidly as it moved forward over the WNP. Around 2100 UTC 2 October, Fitow reached typhoon strength with maximum sustained winds of 30 m/s. At 0900 UTC 4 October, it rapidly became a strong typhoon. Fitow later turned more to the west-north-west, sweeping over the Ryukyu Islands with a peak wind speed of 38 m/s on 5 October. At 1715 UTC 6 October, Fitow landed at Fuding, a city in Fujian, with a landfall pressure of 955 hPa and maximum wind speed of 42 m/s, but then quickly weakened over land, dissipating at 0100 UTC 7 October.

Fitow was the strongest typhoon that struck China in October from 1949 to 2013 and caused severe damage (urban water logging, flooding, and debris flow disasters) to Zhejiang province due to its torrential rainfall and wind gusts during 6–8 October 2013 (Yu et al., 2014; Bao et al., 2015; Xu and Du, 2015; Lou and Li, 2016; Xu and Li, 2017).

2.2 Validation data

The rainfall validation data released by the Chinese Meteorological Data Sharing Service System has a spatial resolution of 0.1° × 0.1° and a spatial coverage of 70°E–140°E, 15°N–60°N. The hourly precipitation fusion product was obtained by merging observational data from automatic weather stations (AWS) and CPC morphing technique (CMORPH) retrieved satellite data. The probability density matching and optimal interpolation data fusion algorithm were applied to generate the precipitation fusion products. The hourly observational precipitation data are taken from over 30 thousand AWS across China after quality control (Xu et al., 2016). The CMORPH satellite inversion precipitation products were released by the National Oceanic and Atmospheric Administration (NOAA) with a temporal resolution of 0.5 h and a spatial resolution of 8 km, respectively. The rainfall validation data has been widely evaluated in China's mainland, and has been validated for the simulations of typhoon events (Yu et al., 2009).

3 Method

3.1 Model configuration and optimization

A fully compressible non-hydrostatic mesoscale model, the advanced research version of the weather research and prediction (WRF-ARW) model version 3.6.1, is used for this study (Skamarock and Klemp, 2008). Our model configuration uses a single 10-km-mesh domain with 174 × 130 grid points and 36 vertical levels. The model top is set at 10 hPa in a stretched vertical grid. The Yonsei University planetary boundary scheme (Hong et al., 2006), the Rapid Radiative Transfer Model (RRTM) for shortwave and longwave radiation processes (Iacono et al., 2008), the revised Monin-Obukhov surface layer scheme (Jiménez et al., 2012), and the five-layer thermal diffusion Noah land surface model (Chen and Dudhaia, 2001) are applied. For the CPS, the following three experiments are designed: 1) the KF (Kain and Fritsch, 1990; Kain, 2004) scheme with default parameter values (experiment STKF), 2) the KF scheme with optimizing parameter values with micro-GA (experiment OPKF) and 3) no CP scheme (experiment NOCP). The 6-hourly lateral boundary conditions for the WRF model are given by the NCEP Global Final Analysis (FNL) data with 1° × 1° horizontal

resolution.

Considering the combined effect of the CPS and MPS on precipitation prediction in the WRF model, to optimize the simulation and clarify the effect of the CP optimization process, the optimization of MPSs is determined first according to the QPF skill (Equitable Threat Score (*ETS*), see Section 3.4) from control experiments which are carried using five different MPSs. The MPSs used in the control experiments and the corresponding *ETS* values of each precipitation simulation are listed in Table 1. Then, according to the maximum *ETS* value, the Thompson scheme (Thompson et al., 2004) is employed for Meranti and the Lin scheme (Lin et al., 1983) for Fitow. Therefore, using the optimal MPS obtained through the control experiments, the improvement in QPF skill after the subsequent optimization process will be contributed by the optimized CPS. For each case, the effectiveness of the optimization algorithm can be proved as long as the configuration remains unchanged except for CPS to be optimized.

Table 1 ETS scores of two typhoon precipitation cases for different microphysics schemes

Microphysics scheme	*ETS* (Meranti)	*ETS* (Fitow)
Lin	1.9555	2.17932
WSM6	1.71965	2.08121
Thompson	1.99615	1.68166
Morrison 2-mom	1.78405	2.02261
WDM6	1.71965	2.06245

3.2 Kain-Fritsch cumulus parameterization description

The KF convective parameterization scheme has been used successfully in various models (MM5, Wang and Seaman, 1997; WRF, Skamarock and Klemp, 2008; MPAS, Skamarock et al., 2012). The KF scheme is a mass flux parameterization and uses the Lagrangian parcel method. It can be separated into three parts: 1) the convective trigger function, 2) the mass flux formulation, and 3) the closure assumptions. The KF scheme hypothesize that at least 90% of the convective effective potential energy (CAPE) is lost to stabilize the atmosphere over the time T_{con}, and the amount of CAPE is independent of the grid spacing. Fritsch and Chappell (1980) proposed a technique for estimating the value of T_{con} from the mean tropospheric horizontal wind speed and grid resolution, basing on the advective time scale (T_{adv}) in the cloud layer with the constraint range of 1800 to 3600 s. The advective time scale in the KF CPS is defined as follows:

$$T_{\mathrm{adv}} = \frac{\Delta x}{0.5(V_{500} + V_{\mathrm{lcl}})}, \tag{1}$$

where V_{500} is the wind speed (m/s) at 500 hPa, V_{lcl} is the wind speed at the lifting condensation level (LCL), and Δx is the grid spacing (m).

Then T_{con} can be defined as

$$T_{\mathrm{con}} = \begin{cases} 3600\ \mathrm{s} & T_{\mathrm{adv}} > 3600\ \mathrm{s} \\ T_{\mathrm{adv}} & 1800\ \mathrm{s} < T_{\mathrm{adv}} < 3600\ \mathrm{s} \\ 1800\ \mathrm{s} & T_{\mathrm{adv}} < 1800\ \mathrm{s} \end{cases}. \tag{2}$$

Considering that KF scheme was originally designed for a mesoscale model with grid scale of 20–50 km, this formulation may have limitations for either high-resolution grids or strong wind environments such as hurricane simulations. As we move from coarser- to finer-resolution grids, T_{con} should decrease with increased grid resolution to make the scheme seamless across these spatial scales. However, according to the current KF scheme formulation, when the grid spacing decreases the convective time scale stays at a minimum prescribed value of 1800 s. This will cause the updrafts and consequent precipitation amounts to be unrealistically strong at fine grid resolutions (Bullock et al., 2015).

The grid-scale rainfall is dependent on the hydrometeor feedback, which is affected by the conversion rate. The amount of condensate lost (δr_{c}) by the updraft in a given layer, δ_z, is specified in the KF parameterization as

$$\delta r_{\mathrm{c}} = \gamma_{\mathrm{co}}\left(1.0 - \exp^{-\frac{c\delta_z}{\omega}}\right), \tag{3}$$

where γ_{co} is the condensate at the bottom of the layer, cis the conversion rate, and ω is the updraft vertical velocity. The constant c directly affects the hydrometeor feedback that reduces the convective precipitation. A large c value is associated with convective precipitation whereas a small c value is associated with non-convective precipitation. Therefore, as the grid spacing decreases, more of the restoration of atmospheric stability is performed by the grid-scale cloud microphysics scheme, so the conversion rate decreases (Sims et al., 2017).

3.3 Micro-GA algorithm

The genetic algorithm is a parallel stochastic optimization search method that simulates the genetic mechanism and biological evolution of nature. It is a heuristic global search optimization method based on the laws of natural selection in which the most suitable solution survives while inferior solutions are eliminated. The parameter value selection problem can be considered to be a configuration of parameters as a chromosome with one-to-one mapping between genes and parameter values (Oana and Spataru, 2017).

The three critical processes in GA are selection, crossover, and mutation (Haidar and Verma, 2017). Selection is the process of choosing individuals from a

population based on their fitness to reproduce the next population. Crossover is a GA operator that selects genes from parent chromosomes and creates a new offspring. Mutation includes random transformation of values of genes in the chromosome. The operators are used to screen individuals, keeping individuals with good fitness, weeding out poor ones, and preserving not only the information of the previous generation of individuals in the new population, but also making the new population superior to the previous generation.

The most common type of genetic algorithm works as follows: a population is created with a randomly generated set of individuals (represented by chromosomes). Individuals in the population are then assessed by fitness function, which assign scores to individuals based on their performance in a given task. The higher the score, the more suitable they are, and the greater chance they have to reproduce. The evolution process continues until some condition (e.g., improvement of the best solution or a certain number of generations have passed) is satisfied. The procedural details of genetic algorithms can be found in Szpiro (1997), Álvarez et al. (2000), Jin and Wang (2001), and Kishtawal et al. (2003).

The micro-GA proposed by Krishnakumar (1990) does not include mutation because diversifying a small population will not represent the solution space well. Since micro-GA uses a special sampling technique, it can converge to a local maximum (pseudo-convergence). To avoid pseudo-convergence, the system allows re-initialization based on random selection when it converges to either a local or global maximum, but the elite individual from the previous iteration is retained (Hong et al., 2006). The solutions diversity is achieved by starting with a new randomly generated population while maintaining the best solution previously obtained.

3.4 Fitness function

Since the evaluation procedure is a critical part of the genetic algorithm optimization and only one fitness function is used in micro-GA, it is obviously necessary to select an appropriate fitness function (Hong et al., 2015). As our experiments focus on forecasting precipitation, the *ETS* is chosen as the fitness function to be optimized in the genetic algorithm, which is known as a skill score for QPF. The *ETS* indicates the ability of numerical models to predict precipitation by comparing predicted precipitation with observational precipitation products, and the fitness function is defined as follows:

$$\text{Fitness} = \Sigma_i ETS_i,$$

$$i = 10,\ 25,\ 50,\ 75,\ldots,\ 300,\ 350, \tag{4}$$

where i is the precipitation threshold in millimeters. Each *ETS* is calculated as follows (Schaefer, 1990; Clark et al., 2007; Wang, 2014):

$$ETS_i = \frac{H-R}{F+O-H-R},$$

$$R = F\frac{O}{N}, \tag{5}$$

where F and O represent the number of grid points at which the rainfall amount is greater than the specified precipitation threshold for forecast and observation, respectively; H is the number of samples correctly forecast to exceed the threshold; R is the number of fortuitous correct forecasts; and N is the total number of points being verified. R can be determined by using the event frequency (O/N) multiplied by the number of forecasts of event occurrence (F) (Brill and Mesinger, 2009). *ETS* values can range from –1/3 to 1, where a score of 1 is perfect while scores below 0 mean it is worse than a random forecast, and $ETS = 0$ indicates the forecast is random.

3.5 Optimization process of the WRF-micro-GA system

The coupling of WRF and micro-GA for the optimization process is represented in the algorithm flow chart (Fig. 2) through the following steps. 1) The micro-GA generates a random population of n chromosomes when the algorithm is initialized. The information represented by the solution should be contained in some way (such as binary coding) by the chromosome. 2) Micro-GA integrates a series of WRF runs by applying each scheme combination to the KF scheme source code modification in WRF. 3) During the series run, the fitness function is used to evaluate the simulation in comparison with observational data, and the selected scheme combination is inherited to the offspring generation through the crossover mechanism. 4) The processes above continue until the optimal value is reached when the entire iteration converges to the global maximum (Hong et al., 2015). In this study, the population size was set to 5, the evolutionary generation was set to 100 and a crossover rate of 0.5 was applied for both experiments.

4 Results and discussion

4.1 Improvement in QPF skill

The WRF-micro-GA scheme has been applied to optimize two parameters (T_{con} and c) in the KF scheme to enhance the skill of QPF. Figure 3 depicts the evolution of the fitness function with each generation of the micro-GA. The optimized values for the precipitation forecasts of Meranti and Fitow are obtained in about 40 generations and 90 generations, respectively, indicating that the micro-GA has the ability to find the maximum fitness function. The optimized values of parameter T_{con} are about 1680 s for

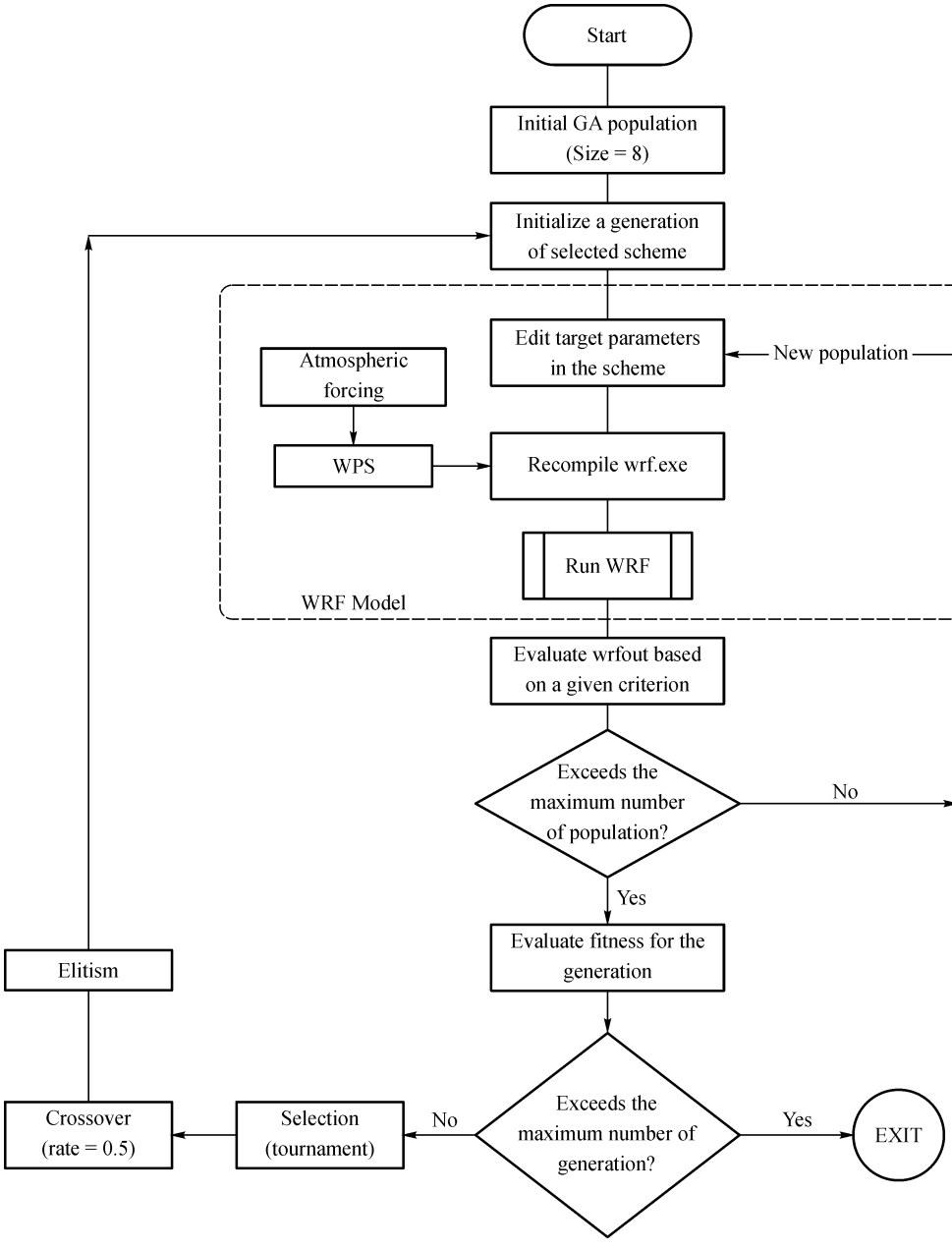

Fig. 2 The WRF-micro-GA system flow chart, showing the coupling of the KF scheme in the WRF model with the micro-GA.

Meranti and 690 s for Fitow, illustrating that the convective time scales may not be bounded by 1800 s for high resolutions such as 10 km. The T_{con} value is related to the selection of MPS, which affects the value of LCL and V_{lcl} in Eq. (1). An additional experiment was conducted to set MPS as Lin scheme (Lin et al., 1983), and the T_{con} value was optimized to 750 s. The optimized values of the parameter are about 0.0148/s for Meranti and 0.0022/s for Fitow, smaller than the standard 0.03/s in the KF scheme source code in WRF. A smaller c implies an increase in sub-grid condensed cloud water at the cost of convective precipitation.

Figure 4 shows the *ETS*s for the respective precipitation thresholds (unit: mm) of the three experiments (NOCP, STKF, and OPKF) for each case. It demonstrates that the *ETS*s with OPKF simulations are generally higher than those with NOCP and STKF. Significant improvements in QPF are evident with an increase in *ETS* by 5.8% for the Meranti case, and by 18.4% for the Fitow case. For Meranti, the OPKF shows a slight improvement for thresholds of 50 to 220 in QPF compared with the STKF experiment. Both the OPKF and STKF simulations perform better than NOCP at thresholds higher than 50 mm/d. For Fitow, the QPF improves significantly in the OPKF experiment at a threshold range of 10–170 mm/d, but deteriorates at thresholds higher than 170 mm/d

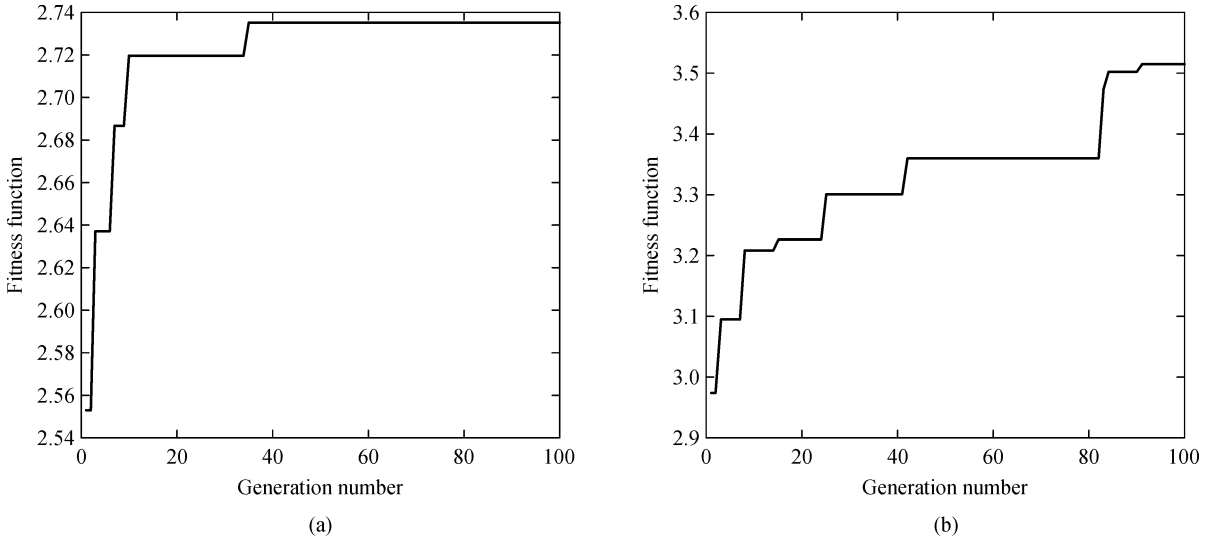

Fig. 3 The fitness function of each generation for (a) Meranti, (b) Fitow.

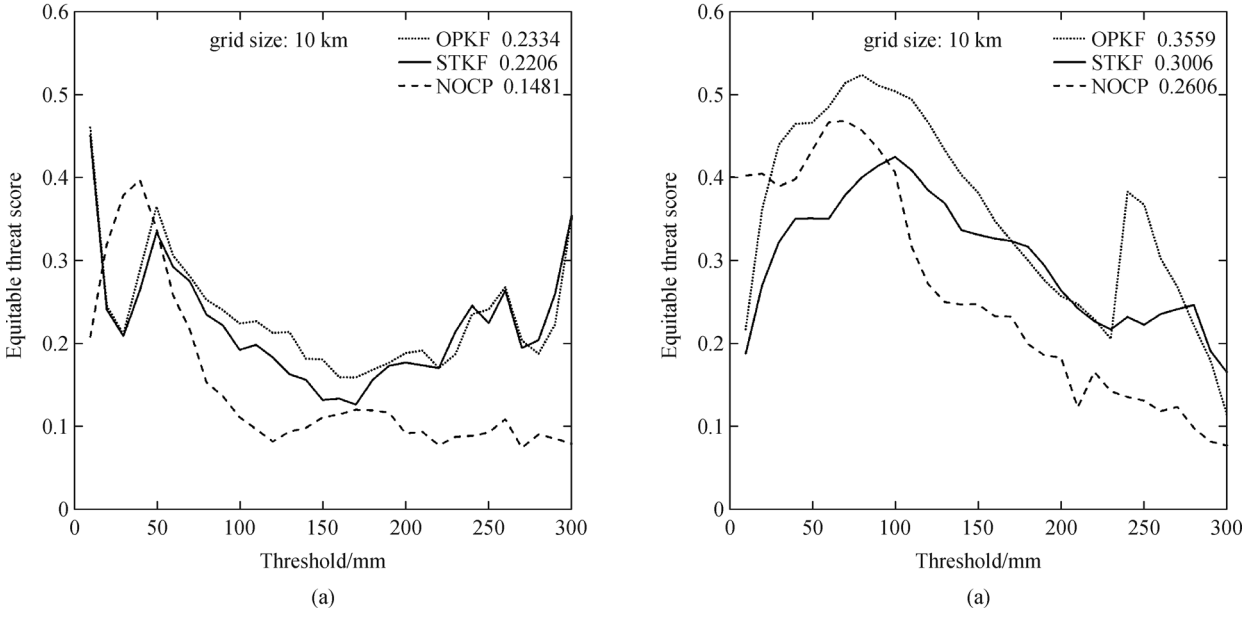

Fig. 4 *ETS* values for various rainfall thresholds (unit: mm) for (a) Meranti and (b) Fitow. The numbers beside the experiment names are the averaged *ETS*.

compared with the STKF experiment. However, the forecast skill of the OPKF experiment is clearly better than that of the NOCP experiment at most thresholds (from about 30 to 270 mm/d. In addition, the STKF experiment performs better than NOCP for thresholds of about 100 to 300 mm/d. On the whole, precipitation skill scores have improved.

4.2 Spatial distribution of simulated precipitation

The 24-h accumulated precipitation observed for Typhoon Meranti is shown in Fig. 5(a) and for Typhoon Fitow in Fig. 6(a). The periods are from 1000 UTC 14 September 2016 to 1000 UTC 15 September 2016 for Meranti, and from 1200 UTC 6 October to 1200 UTC 7 October for Fitow. For Meranti, the observed torrential rainfall occurred along the eastern coastal areas (location A and B). For Fitow, the observed torrential rainfall occurs along the coastal areas with a rainband in the north that is oriented northwest-southeast from Anji city to Ningbo city (location D) and two rainfall centers located in the east (location E).

The model was used to simulate the typhoons for 36 h with the pre-selected MPSs set out in Section 3.1. Treating

the first 12-h simulation as spin-up, and the subsequent 24-h simulation were used for the analysis of rainfall partitioning. Figures 5(b)–5(d) and 6(b)–6(d) show the simulated 24-h (corresponding to the observational period) accumulated precipitation from the control experiments (NOCP, STKF, and OPKF).

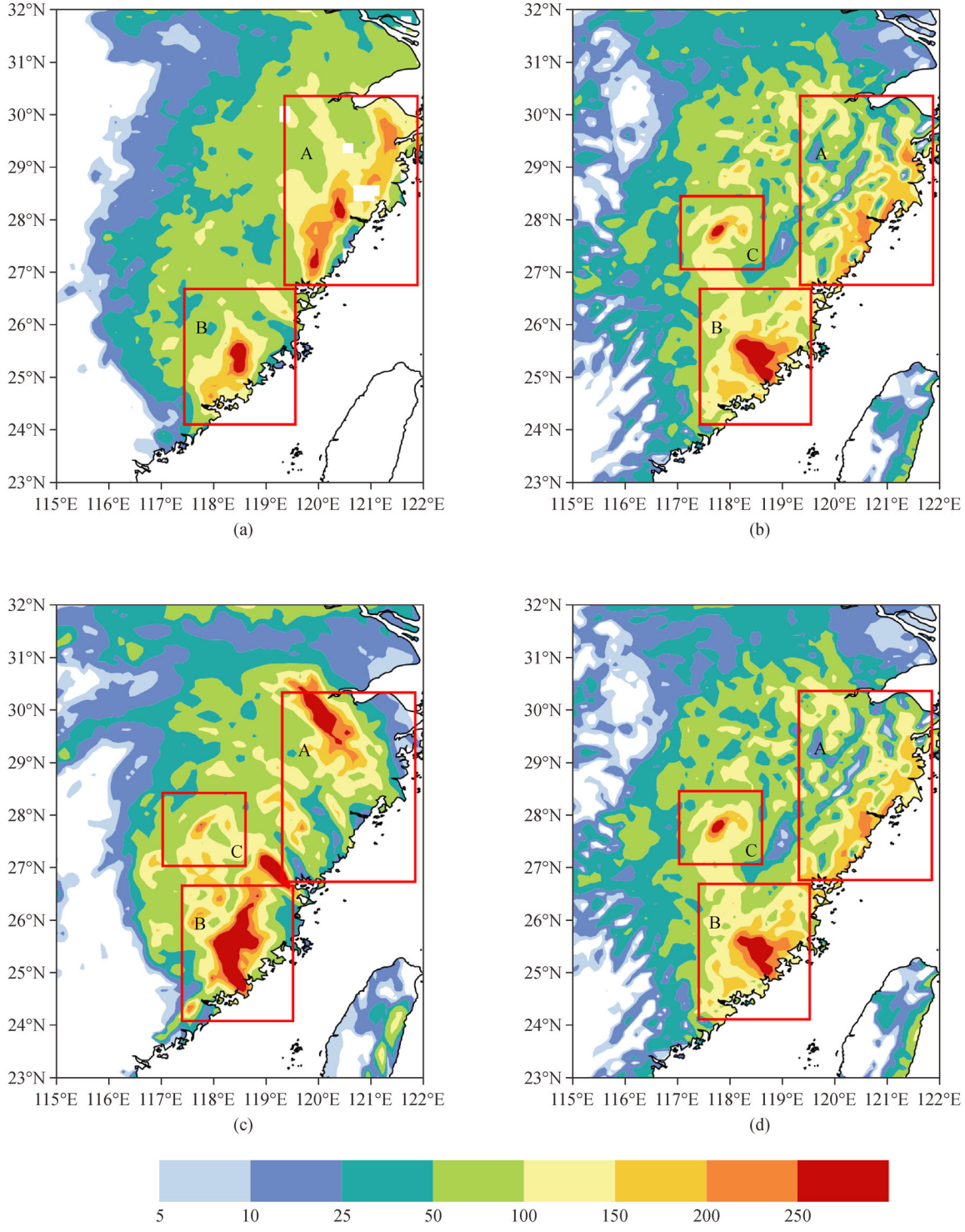

Fig. 5 Horizontal distribution of 24 h accumulated rainfall (unit: mm) caused by Typhoon Meranti from 1000 UTC 14 September 2016 to 1000 UTC 15 September 2017 for (a) observations, (b) OPKF, (c) NOCP, and (d) STKF.

For Meranti, the OPKF (Fig. 5(b)) simulated the strong rainband along the east coast (location A) and the heavy rain zone (location B) is close to that observed. However, there is a spurious precipitation maximum (>200 mm/d) in the north-western area (location C). In addition, the rainfall in the south region is relatively large and the precipitation area in north central region is not continuous enough. The STKF (Fig. 5(d)) simulation is similar to the OPKF simulation, although the simulation of rainfall intensity is not quite as accurate (the strong rainband in location A is weaker). For the NOCP (Fig. 5(c)) experiment, the strong rainband along the location A is not captured but an area of spurious heavy rainfall occurs in the northwest. The rainband (threshold larger than 200 mm/d) along the east coast (location B) is spurious and the simulated precipitation over the south region is generally too high.

For Fitow, the OPKF (Fig. 6(b)) simulated the northwest-southeast rainband, but it appears to the south of that observed. Xu and Du (2015) made a diagnosis of the heavy rainfall caused by Fitow (2013); their results pointed out that extra moisture brought by Typhoon Danas (2013)

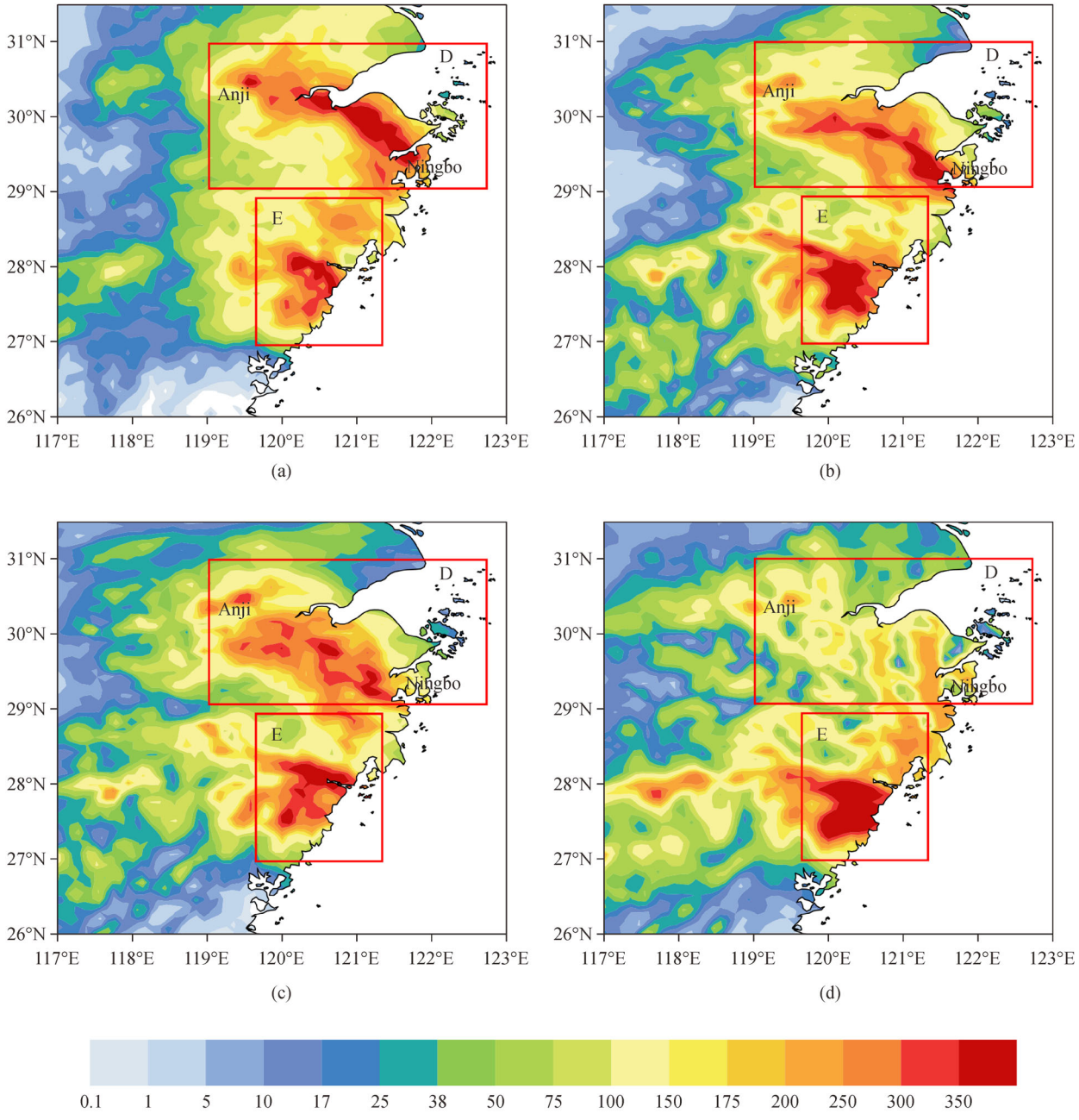

Fig. 6 Horizontal distribution of 24 h accumulated rainfall (unit: mm) caused by Typhoon Fitow from 1200 UTC 06 October 2013 to 1200 UTC 07 October 2013 for (a) observations, (b) OPKF, (c) NOCP, and (d) STKF.

played an important role in maintaining and enhancing the north rainband of Fitow, resulting in torrential rainfall over northern area (location D). Computational resources limited the extent of the simulation, so the simulated area is too small and the period too short to include typhoon Danas (Fig. 1(b)), which might explain why the rainband in northern area is too narrow and shifted to the south. The NOCP (Fig. 6(c)) simulation shows a northwest-southeast rainband without a continuous strong center. The STKF (Fig. 6(d)) simulation does not capture the northwest-southeast rainband, although the east coast rain center (location E) is simulated. All three experiments captured the heavy rainfall area over the southeast coast (location E) but overestimated the rainfall. To sum up, in both cases, OPKF gave the best simulation results.

4.3 Discussion

It is generally recognized that CPSs may not be suitable for high resolution, but the simulations with the STKF scheme performed better than NOCP experiments in Meranti at a resolution of 10 km in this study, which differs from the result in Yu et al. (2013). However, the OPKF experiments can improve the precipitation prediction skills for all the cases simulated with optimized MPSs, thereby illustrating the robustness of the optimization system. Therefore, the use of CPSs is worth exploring at high resolution, particularly if the CPS parameters are optimized.

Even though the *ETS*s did not improve significantly at some thresholds, the forecast skills improved with the optimized parameter values and the simulation of strong precipitation areas is closer to the observations. Therefore, this study further verifies the effectiveness of the WRF-micro-GA method as demonstrated in previous studies.

Due to the limitations of the *ETS* scoring method, it is suggested that a more suitable testing scoring method for rainstorm forecasting be selected as the fitness function in future studies, so as to further improve the precipitation prediction skills. The optimized parameter values in this study are consistently smaller than the default values of the model itself. However, in order to obtain more representative parameter values, it is necessary to investigate more individual typhoon cases and obtain the optimized parameter values for different typhoon types through typhoon cluster analysis. Also, a higher resolution can be set to capture the localized and sub-grid features. Considering that the original values were estimated based on empirical formulas or limited observations, more effort can be put into improving the physical and dynamical processes in the model. The micro-GA method is stable and effective. The typhoon quantitative precipitation forecast skills can be improved by choosing *ETS*s as the fitness function. Otherwise, the prediction of typhoon tracks and intensity can also be improved with the parameters in physical schemes optimized with different fitness functions.

Acknowledgements This study was financially supported by the National Basic Research Program of China (Grant No. 2015CB452806). The computation was supported by the ECNU Multifunctional Platform for Innovation (001).

References

Arakawa A (2004). The cumulus parameterization problem: Past, present, and future. J Clim, 17(13): 2493–2525

Aybar-Ruiz A, Jiménez-Fernández S, Cornejo-Bueno L, Casanova-Mateo C, Sanz-Justo J, Salvador-González P, Salcedo-Sanz S (2016). A novel grouping genetic algorithm–extreme learning machine approach for global solar radiation prediction from numerical weather models inputs. Sol Energy, 132: 129–142

Álvarez A, López C, Riera M, Hernández-García E, Tintoré J (2000). Forecasting the sst space-time variability of the Alboran Sea with genetic algorithms. Geophys Res Lett, 27(17): 2709–2712

Bao X, Davidson N E, Yu H, Hankinson M C N, Sun Z, Rikus L J, Liu J, Yu Z, Wu D (2015). Diagnostics for an extreme rain event near Shanghai during the landfall of Typhoon Fitow (2013). Mon Weather Rev, 143(9): 3377–3405

Bauer P, Thorpe A, Brunet G (2015). The quiet revolution of numerical weather prediction. Nature, 525(7567): 47–55

Brill K F, Mesinger F (2009). Applying a general analytic method for assessing bias sensitivity to bias-adjusted threat and equitable threat scores. Weather Forecast, 24(6): 1748–1754

Bullock O R Jr, Alapaty K, Herwehe J A, Kain J S (2015). A dynamically computed convective time scale for the Kain-Fritsch convective parameterization scheme. Mon Weather Rev, 143(6): 2105–2120

Chen F, Dudhia J (2001). Coupling an advanced land surface-hydrology model with the penn state-ncar mm5 modeling system. Part I: model implementation and sensitivity. Mon Weather Rev, 129(4): 569–585

Clark A J, Gallus W A Jr, Chen T C (2007). Comparison of the diurnal precipitation cycle in convection-resolving and non-convection resolving mesoscale models. Mon Weather Rev, 135(10): 3456–3473

Correia J Jr, Arritt R W, Anderson C J (2008). Idealized mesoscale convective system structure and propagation using convective parameterization. Mon Weather Rev, 136(7): 2422–2442

Dai A (2006). Precipitation characteristics in eighteen coupled climate models. J Clim, 19(18): 4605–4630

Davis C A, Bosart L F (2002). Numerical simulations of the genesis of Hurricane Diana (1984). Part II: sensitivity of track and intensity prediction. Mon Weather Rev, 130(5): 1100–1124

Fritsch J M, Chappell C F (1980). Numerical prediction of convectively driven mesoscale pressure systems. Part I: convective parameterization. J Atmos Sci, 37(8): 1722–1733

Haidar A, Verma B (2017). A genetic algorithm based feature selection approach for rainfall forecasting in sugarcane areas. Computational Intelligence. IEEE

Hong S, Park S K, Yu X (2015). Scheme based optimization of land surface model using a micro-genetic algorithm: assessment of its performance and usability for regional applications. Sci Online Lett Atmos, 11: 129–133

Hong S Y, Noh Y, Dudhia J (2006). A new vertical diffusion package

with an explicit treatment of entrainment processes. Mon Weather Rev, 134(9): 2318–2341

Iacono M J, Delamere J S, Mlawer E J, Shephard M W, Clough S A, Collins W D (2008). Radiative forcing by long-lived greenhouse gases: calculations with the AER radiative transfer models. J Geophys Res D Atmos, 113(D13): D13103

Jiménez P A, Dudhia J, González-Rouco J F, Navarro J, Montávez J P, García-Bustamante E (2012). A revised scheme for the WRF surface layer formulation. Mon Weather Rev, 140(3): 898–918

Jin Y Q, Wang Y (2001). A genetic algorithm to simultaneously retrieve land surface roughness and soil wetness. Int J Remote Sens, 22(16): 3093–3099

Kishtawal C M, Basu S, Patadia F, Thapliyal P K (2003). Forecasting summer rainfall over India using genetic algorithm. Geophys Res Lett, 30(23): 2203

Kain J S, Fritsch J M (1990). A one-dimensional entraining/detraining plume model and its application in convective parameterization. J Atmos Sci, 47(23): 2784–2802

Kain J S (2004). The Kain-Fritsch convective parameterization: an update. J Appl Meteorol, 43(1): 170–181

Krishnakumar K (1990). Micro-genetic algorithms for stationary and non-stationary function optimization. In: Intelligent Control and Adaptive Systems, 1196: 289–296

Lee Y H, Park S K, Chang D E (2006). Parameter estimation using the genetic algorithm and its impact on quantitative precipitation forecast. Ann Geophys, 24(12): 3185–3189

Li F, Song J, Li X (2018). A preliminary evaluation of the necessity of using a cumulus parameterization scheme in high-resolution simulations of typhoon Haiyan (2013). Nat Hazards, 92(2): 647–671

Li M, Ping F, Tang X, Yang S (2019). Effects of microphysical processes on the rapid intensification of Super Typhoon Meranti. Atmos Res, 219: 77–94

Li X (2013). Sensitivity of WRF simulated typhoon track and intensity over the Northwest Pacific Ocean to cumulus schemes. Sci China Earth Sci, 56(2): 270–281

Li X, Pu Z (2009). Sensitivity of numerical simulations of the early rapid intensification of Hurricane Emily to cumulus parameterization schemes in different model horizontal resolutions. J Meteorol Soc Jpn, 87(3): 403–421

Liang X Z, Xu M, Kunkel K E, Grell G A, Kain J S (2007). Regional climate model simulation of U.S.-Mexico summer precipitation using the optimal ensemble of two cumulus parameterizations. J Clim, 20 (20): 5201–5207

Lin Y, Farley R D, Orville H D (1983). Bulk parameterization of the snow field in a cloud model. J Clim Appl Meteorol, 22(6): 1065–1092

Lou L, Li X (2016). Radiative effects on torrential rainfall during the landfall of Typhoon Fitow (2013). Adv Atmos Sci, 33(1): 101–109

Neggers R A J, Siebesma A P, Lenderink G, Holtslag A A M (2004). An evaluation of mass flux closures for diurnal cycles of shallow cumulus. Mon Weather Rev, 132(11): 2525–2538

Oana L, Spataru A (2017). Use of genetic algorithms in numerical weather prediction. In: 18th International Symposium on Symbolic and Numeric Algorithms for Scientific Computing (SYNASC). 2016: 456–461

Qiao F, Liang X Z (2016). Effects of cumulus parameterization closures on simulations of summer precipitation over the United States coastal oceans. J Adv Model Earth Syst, 8(2): 764–785

Sandeep C P R, Krishnamoorthy C, Balaji C (2018). Impact of cloud parameterization schemes on the simulation of Cyclone Vardah using the WRF model. Curr Sci, 115(6): 1143–1153

Schaefer J T (1990). The critical success index as an indicator of warning skill. Weather Forecast, 5(4): 570–575

Sims A P, Alapaty K, Raman S (2017). Sensitivities of summertime mesoscale circulations in the coastal Carolinas to modifications of the Kain-Kritsch cumulus parameterization. Mon Weather Rev, 145(11): 4381–4399

Singh R, Singh C, Ojha S P, Kumar A S, Kishtawal C M, Kumar A S K (2016). Land surface temperature from INSAT-3D imager data: retrieval and assimilation in NWP model. J Geophys Res D Atmospheres, 121(12): 6909–6926

Skamarock W C, Klemp J B (2008). A time-split nonhydrostatic atmospheric model for weather research and forecasting applications. J Comput Phys, 227(7): 3465–3485

Skamarock W C, Klemp J B, Duda M G, Fowler L D, Park S H, Ringler T D (2012). A multiscale nonhydrostatic atmospheric model using centroidal voronoi tesselations and c-grid staggering. Mon Weather Rev, 140(9): 3090–3105

Sugimoto S, Takahashi H G (2016). Effect of spatial resolution and cumulus parameterization on simulated precipitation over South Asia. Sola, 12(Special Edition): 7–12

Sun Y, Zhong Z, Lu W, Hu Y (2014). Why are tropical cyclone tracks over the western north pacific sensitive to the cumulus parameterization scheme in regional climate modeling—a case study for Megi (2010). Mon Weather Rev, 142(3): 1240–1249

Szpiro G G (1997). Forecasting chaotic time series with genetic algorithms. Phys Rev E, 55(3): 2557–2568

Thompson G, Rasmussen R M, Manning K (2004). Explicit forecasts of winter precipitation using an improve bulk microphysics scheme. Part I: description and sensitivity analysis. Mon Weather Rev, 132(2): 519–542

Wang W, Seaman N L (1997). A comparison study of convective parameterization schemes in a mesoscale model. Mon Weather Rev, 125(2): 252–278

Wang C C (2014). On the calculation and correction of equitable threat score for model quantitative precipitation forecasts for small verification areas: the example of Taiwan. Weather Forecast, 29(4): 788–798

Xu H, Du B (2015). The impact of Typhoon Danas (2013) on the torrential rainfall associated with Typhoon Fitow (2013) in east China. Adv Meteorol, 2015: 1–11

Xu H, Liu R, Zhai G, Li X (2016). Torrential rainfall responses of typhoon Fitow (2013) to radiative processes: a three-dimensional WRF modeling study. J Geophys Res D Atmospheres, 121(23): 14127–14136

Xu H, Li X (2017). Torrential rainfall processes associated with a landfall of Typhoon Fitow (2013): a three-dimensional wrf modeling study. J Geophys Res D Atmospheres, 122(11): 6004–6024

Yang M J, Tung Q C (2003). Evaluation of rainfall forecasts over Taiwan by four cumulus parameterization schemes. J Meteorol Soc Jpn, 81 (5): 1163–1183

Yu X, Park S K, Lee Y H, Choi Y S (2013). Quantitative precipitation

forecast of a tropical cyclone through optimal parameter estimation in a convective parameterization. Sci Online Lett Atmos, 9(0): 36–39

Yu Z, Yu H, Chen P, Qian C, Yue C (2009). Verification of tropical cyclone related satellite precipitation estimates in mainland China. J Appl Meteorol Climatol, 48(11): 2227–2241

Yu Z F, Chen Y D, Wu D, Chen G M, Bao X W, Uamg Q Z, Yu R L, Zhang L, Tang J, Xu M, Zeng Z J (2014). Overview of Severe Typhoon Fitow and its operational forecasts. Trop Cyclone Res Rev, 3: 22–34

Zhang C, Wang Y (2018). Why is the simulated climatology of tropical cyclones so sensitive to the choice of cumulus parameterization scheme in the WRF model? Clim Dyn, 51(9–10): 3613–3633

Zheng Y, Alapaty K, Herwehe J A, Del Genio A D, Niyogi D (2016). Improving high-resolution weather forecasts using the weather research and forecasting (WRF) model with an updated Kain-Fritsch scheme. Mon Weather Rev, 144(3): 833–860